Generalized Flexible Method for Simulating Transient Pipe Network Hydraulics

J. D. Nault[1]; B. W. Karney, M.ASCE[2]; and B.-S. Jung[3]

Abstract: Characteristic solution methods, namely the method of characteristics (MOC) and wave characteristics method (WCM), are widely used for simulating transient pipe network flows. Because the MOC computes solutions at interior nodes, it features higher spatial resolution, whereas the WCM makes simplifications that yield more efficient computations. Practical analyses require numerical methods that are both accurate and computationally efficient. To benefit from the advantages of the two approaches, a generalized characteristic method (GCM) is developed in this paper by combining a flexible friction approximation with a variable reach scheme. Significantly, computational savings are realized by selectively providing greater accuracy and higher resolution solutions only where needed via more interior reaches and higher order solutions; further, the new method reduces to either of the MOC and WCM, thereby showing their intrinsic similarities. Multiple examples compare and contrast the numerical methods. From these, unsteady friction effects and, more importantly, spatial resolution are shown to be directly affected by the interior reach treatment, thus exposing a limitation for solution methods with too few interior reaches. Overall, the key contribution of this work is a methodology featuring a similar degree of accuracy to the MOC, but with a computational cost better than that of the WCM. **DOI: 10.1061/(ASCE)HY.1943-7900.0001432.** © *2018 American Society of Civil Engineers.*

Author keywords: Water hammer; Method of characteristics; Wave characteristics method; Hydraulic models; Transient flow; Pipe networks; Water distribution systems.

Introduction

Water pipe systems are designed and operated to meet specific hydraulic requirements for pressure and flow. One particular challenge concerns these properties under transient flow conditions, which arise due to changes at the boundaries of a system (e.g., pump and valve operations). The extreme pressures resulting from rapid changes can lead to pipe breaks, component failure, and contaminant intrusion (Boyd et al. 2004; Friedman et al. 2004), so there is an ever-present need for hydraulic transient analysis via numerical modeling. Though important, models are computationally demanding.

Fundamental to unsteady flow modeling and thus efficient analysis is the numerical solution of the governing water hammer equations. Various approaches have been developed for pipe networks, including Eulerian time domain (Chaudhry and Hussaini 1985; Zhao and Ghidaoui 2004; León et al. 2008; Chaudhry 2014), Lagrangian time domain (Ferrante et al. 2009; Huang et al. 2017), and frequency domain schemes (Wylie and Streeter 1993; Kim 2007; Zecchin et al. 2010; Vítkovský et al. 2011). Among these, the Eulerian method of characteristics (MOC) (Wylie and Streeter 1978) and the Lagrangian wave characteristics method (WCM) (Wood et al. 1966) remain the preferred time-domain alternatives due to their ease of implementation, accurate resolution of shock fronts, and ability to handle complex boundary conditions. By considering interior pipe hydraulics, the MOC yields higher resolution solutions; in contrast, the WCM is more efficient because of its underlying simplifications, a key advantage for large pipe networks. Algebraic water hammer (AWH) (Wylie and Streeter 1993; Nault et al. 2016), a meshless variant of the MOC, represents an even further simplification. Each characteristic approach has a distinct advantage and disadvantage.

Central to modeling are numerical accuracy and computational efficiency. The former is necessary to obtain representative solutions. Computational efficiency pertains more to practical applications, such as problems involving large networks, optimization (Jung et al. 2011), and model calibration (Ebacher et al. 2011). Water distribution system (WDS) analyses, for instance, concern models having thousands to tens-of-thousands of elements. Without efficient solution methods, analyses must compromise on accuracy or performing fewer simulations. For this reason, many studies emphasize the more efficient WCM as a superior alternative to the MOC (Wood 2005; Wood et al. 2005b; Ramalingam et al. 2009), but its efficiency comes at the expense of lower solution resolution. Moreover, there is a trade-off between numerical accuracy and computational efficiency.

To improve model efficiency while balancing the need for numerically accurate solutions, this work generalizes the advantages of the MOC, WCM, and AWH into a flexible unified fixed grid characteristic approach for simulating transient pipe network hydraulics. Central to the generalized characteristic method (GCM) are a flexible friction treatment and a variable reach fixed grid scheme; together, these permit individual pipes to be modeled according to the required solution accuracy. More interior reaches and higher order friction treatments are only provided where needed, maintaining numerical accuracy while yielding efficient computations. Multiple networks of varying complexity demonstrate the

[1]Hydraulic Specialist, HydraTek & Associates, Vaughan, ON, Canada L4L 8S5; formerly, Ph.D. Candidate, Dept. of Civil Engineering, Univ. of Toronto, Toronto, ON, Canada M5S 1A4 (corresponding author). E-mail: j.nault@hydratek.com

[2]Professor, Dept. of Civil Engineering, Univ. of Toronto, Toronto, ON, Canada M5S 1A4. E-mail: karney@ecf.utoronto.ca

[3]Discipline Specialist, Tebodin, P.O. Box 2652, Abu Dhabi, United Arab Emirates. E-mail: paul.jung@tebodin.com

Note. This manuscript was submitted on April 3, 2017; approved on September 18, 2017; published online on April 19, 2018. Discussion period open until September 19, 2018; separate discussions must be submitted for individual papers. This paper is part of the ***Journal of Hydraulic Engineering***, © ASCE, ISSN 0733-9429.

current work. In each case, the GCM features modest to substantial computational savings, comparable numerical accuracy and, moreover, greater flexibility than any individual method on its own. Ultimately these developments benefit practical analyses of transient pipe network hydraulics.

Unsteady Flow Modeling

In formulating the generalized solution, one begins with the characteristic representation of the governing equations. Approximations to the friction integrals are then introduced, and they are combined with the characteristic expressions to assemble a set of compatibility equations that form the solution basis of the GCM.

Governing Equations and Characteristic Lines

One-dimensional unsteady pressurized flow is mathematically described by a pair of nonlinear hyperbolic partial differential equations. The momentum equation

$$\frac{1}{gA}\frac{\partial Q}{\partial t}+\frac{\partial H}{\partial x}+J_{QF}+J_{UF}=0 \tag{1}$$

$$J_{QF}=\frac{f}{2gDA^2}|Q|Q$$

represents the effects of fluid inertia and viscous resistance, and the continuity equation

$$\frac{a^2}{gA}\frac{\partial Q}{\partial x}+\frac{\partial H}{\partial t}=0 \tag{2}$$

relates to fluid compressibility and conduit elasticity, in which Q = flow (m^3/s); H = head (m); f = friction factor; a = wave speed (m/s); g = acceleration due to gravity (m/s^2); A = pipe area (m^2); D = pipe diameter (m); J_{QF} = quasi-steady friction head loss per unit length; J_{UF} = unsteady friction head loss per unit length; t = time (s); and x = distance along the pipe (m). Derivations and further details can be found in Wylie and Streeter (1993) and Chaudhry (2014).

Characteristic methods transform Eqs. (1) and (2) and then integrate them along the positive and negative characteristic lines [Fig. 1(a)]. This yields the positive compatibility expression

$$B(Q_P-Q_A)+(H_P-H_A)+\int_{x_A}^{x_P}J_{QS}dx+\int_{x_A}^{x_P}J_{US}dx=0 \tag{3}$$

$$B=a/gA$$

and the negative compatibility expression

$$B(Q_P-Q_B)-(H_P-H_B)-\int_{x_B}^{x_P}J_{QS}dx-\int_{x_B}^{x_P}J_{US}dx=0 \tag{4}$$

where subscripts A, B, and P refer to those points shown in Fig. 1(a). Eqs. (3) and (4) are, respectively, valid along the C+ and C− lines; these represent the space-time paths along which pressure waves travel.

By discretizing a pipe into N_0 interior reaches, $2N_0$ characteristic lines and N_0+1 nodes are assembled into a computational grid [Fig. 1(b)]. Each reach has a length $\Delta x=L/N_0$ (m) for a uniform grid. To obtain a stable solution, the discretization must satisfy the Courant–Friederich–Lewy (CFL) criterion

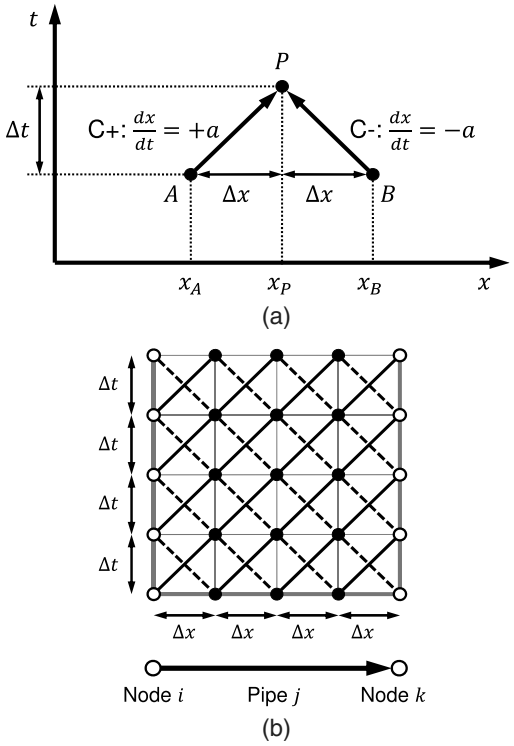

Fig. 1. Characteristic representation of wave space-time paths: (a) positive and negative characteristic lines; (b) characteristic lines and nodes assembled into a space-time computational grid

$$C=a\cdot\frac{\Delta t}{\Delta x}\le 1 \tag{5}$$

where C = Courant number; and Δt = time step (s). Satisfying Eq. (5) for each pipe in a network poses a challenge because individual pipes feature different properties. Using constant Δt, Eulerian approaches require pipe length or wave speed adjustments to satisfy Eq. (5). Interpolation techniques avoid this, although they introduce numerical dispersion. True Lagrangian approaches track wave propagation with variable Δt; however, Δt becomes increasingly smaller as wave propagation frequencies increase for long simulation durations in complex networks, thus impeding computational efficiency (Huang et al. 2017). In this paper, an Eulerian approach is adopted with pipe length and wave speed adjustments. Thus, sufficiently small Δt is needed to minimize any such adjustments. The hydraulics of a discretized pipe are then computed by solving the compatibility expressions using a constant Δt, but first the friction integrals are resolved.

Quasi-Steady Friction Integral Approximations

Viscous fluid resistance is represented by the friction integrals. They are nonlinear, so they can only be solved numerically. In the case of the quasi-steady component, the most common approaches are the first-order explicit and semi-implicit solutions (Wylie 1983), each resulting in linear compatibility equations. While efficient, numerical accuracy and stability also are concerned (see Holloway and Chaudhry 1985; Liou and Wylie 2014).

To maintain generality, a two-coefficient approximation is used for the quasi-steady friction integrals. That for the positive compatibility expression is

$$\int_{x_A}^{x_P} J_{QS} dx \approx \theta K_P |Q_P| Q_P + (1-\theta) K_A (\varepsilon |Q_A| Q_P + (1-\varepsilon) |Q_A| Q_A) \quad (6)$$

$$K_A = \left(\frac{L}{N_R}\right) \frac{f_A}{2gDA^2}, \qquad K_P = \left(\frac{L}{N_R}\right) \frac{f_P}{2gDA^2}$$

and the friction integral for the negative compatibility expression is

$$-\int_{x_B}^{x_P} J_{QS} dx \approx \theta K_P |Q_P| Q_P + (1-\theta) K_B (\varepsilon |Q_B| Q_P + (1-\varepsilon) |Q_B| Q_B) \quad (7)$$

$$K_B = \left(\frac{L}{N_R}\right) \frac{f_B}{2gDA^2}$$

where K = resistance coefficient (s^2/m^5); $0 \le \theta \le 1$ and $0 \le \varepsilon \le 1$ = friction integration parameters; and N_R = number of modeled reaches. The parameter θ represents a weighting between first-order explicit (0) and implicit (1) schemes, where $\theta = 0.5$ yields a second-order approximation. Similarly, $\varepsilon = 0$ corresponds to a first-order explicit solution, but $\varepsilon > 0$ instead gives a semi-implicit approximation. The number of modeled reaches N_R relates to the discretized number of base reaches N_0. Together with θ and ε, N_R forms a key part of the GCM, a topic that is discussed later.

Eqs. (6) and (7) represent the key approximations for characteristic-based methods. Accordingly, their associated numerical error must be controlled to ensure accurate and stable results, and this can be done through the judicious selection of N_R, θ, and ε. A first-order explicit solution with $\theta = \varepsilon = 0$ is often sufficient. However, in cases with coarse computational grids (low N_R), high energy dissipation, or large flow changes, this may not be suitable. Wylie and Streeter's (1993) evaluative index

$$\psi = \frac{R}{N_R} \ll 1, \qquad R = \frac{fL|\bar{Q}|}{2DAa} \quad (8)$$

provides a helpful means of assessing this, where $\bar{Q}$ = representative (often initial) flow (m^3/s). Eq. (8) represents the ratio of the head loss to the potential surge magnitude over a single reach. The attenuation index R characterizes the same but for an entire pipe. A first-order solution typically yields stable results for $\psi \le 0.05 - 0.15$ (Wylie and Streeter 1993); otherwise, a finer discretization (smaller Δt and larger N_R), higher-order solution (with θ or $\varepsilon > 0$), or implicit solution (also with θ or $\varepsilon > 0$) is necessary.

In addition to N_R, θ, and ε, the treatment of f also affects the solution accuracy. The friction factor can be calculated solely based on the initial conditions using the steady friction approach, or it can be updated throughout a simulation according to the flow conditions (the quasi-steady friction approach). When the flow conditions are highly dynamic, unsteady friction effects become important in the response of a system.

Unsteady Energy Dissipation

Unsteady friction is a predominant feature of highly unsteady flows. It arises due to temporal and spatial velocity profile variations, and these typically lead to greater energy dissipation and phase shifts in the frequency response of a system. Numerous unsteady friction models have been developed, from theoretical formulations (Zielke 1968) to more empirical representations (e.g., Brunone et al. 1991). The single coefficient modified instantaneous acceleration-based (MIAB) model of Vítkovský et al. (2006) is considered here due to its wide use in the literature.

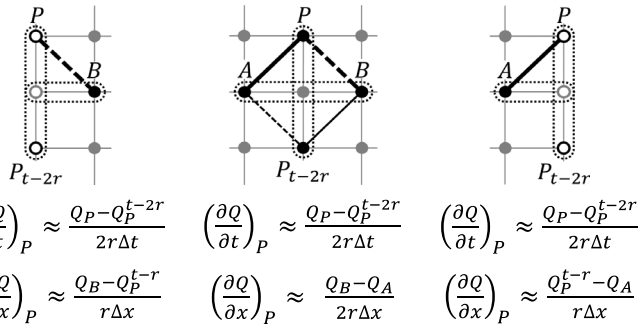

Fig. 2. Finite difference approximations for the modified instantaneous acceleration-based unsteady friction model

Using the MIAB model, the unsteady friction unit head loss term is (Vítkovský et al. 2006)

$$J_{UF} = \frac{k}{gA}\left(\frac{\partial Q}{\partial t} + a \cdot \text{sign}(Q)\left|\frac{\partial Q}{\partial x}\right|\right) \quad (9)$$

where k = shear decay coefficient. The parameter k can be determined experimentally, or it can be estimated empirically as (Vardy and Brown 1996)

$$k = \frac{1}{2}\sqrt{c}, \; c = \begin{cases} 4.76 \times 10^{-3} & \text{Laminar flow} \\ 7.41 \times \mathsf{R}^{-\log_{10}(14.3 \times \mathsf{R}^{-0.05})} & \text{Turbulent flow} \end{cases} \quad (10)$$

where R = Reynolds number.

Eq. (9) can be solved in multiple ways. It can be incorporated into the characteristic transform of the governing equations, or the acceleration terms can be represented using finite difference approximations. In this paper, the latter is used because of its compatibility and stability with staggered computational grids (Fig. 2; see also Vítkovský et al. 2000). Using the scheme in Fig. 2, the unsteady friction integrals for the positive and negative characteristic lines are evaluated as

$$\int_{x_A}^{x_P} J_{UF} dx \approx \frac{1}{2} Bk(Q_P - Q_P^{t-2r} + \text{sign}(Q_A)|Q_B - Q_A|) \quad (11)$$

and

$$-\int_{x_B}^{x_P} J_{UF} dx \approx \frac{1}{2} Bk(Q_P - Q_P^{t-2r} + \text{sign}(Q_B)|Q_B - Q_A|) \quad (12)$$

respectively, in which Q_P^{t-2r} = reach-back flow (m^3/s) at node P from time step $t - 2r$; and $r = N_0/N_R$ is the reach-back index. Together with the compatibility equations and quasi-steady friction integral approximations, the above forms the basis of the generalized characteristic approach.

Generalized Characteristic Method

Compared to the MOC and WCM, the GCM represents a flexible approach to modeling transient pipe network hydraulics. First, the compatibility expressions are evaluated for a fixed grid with the method of specified intervals, and then solutions thereto are obtained. By combining these with a variable reach scheme,

individual pipes are modeled with one or multiple interior reaches to permit flexible and efficient computations.

Compatibility Equations

Using the friction integral approximations and unsteady friction model, the compatibility expressions [Eqs. (3) and (4)] are expanded. For the positive characteristic, combining Eqs. (3), (6), and (11) gives

$$B_A Q_P + H_P - C_A = 0 \tag{13}$$

$$B_A = \left(1 + \frac{1}{2}k\right)B + \theta K_P|Q_P| + (1-\theta)\varepsilon K_A|Q_A|$$

$$C_A = (B - (1-\theta)(1-\varepsilon)K_A|Q_A|)Q_A + H_A + U_A$$

$$U_A = \frac{1}{2}Bk(Q_P^{t-2r} - \text{sign}(Q_A)|Q_B - Q_A|)$$

where B_A = coefficient (s/m^2); and C_A and U_A = constants (m). Similarly, combining Eqs. (4), (7), and (12) for the negative compatibility equation leads to

$$B_B Q_P - H_P - C_B = 0 \tag{14}$$

$$B_B = \left(1 + \frac{1}{2}k\right)B + \theta K_P|Q_P| + (1-\theta)\varepsilon K_B|Q_B|$$

$$C_B = (B - (1-\theta)(1-\varepsilon)K_B|Q_B|)Q_B - H_B + U_B$$

$$U_B = \frac{1}{2}Bk(Q_P^{t-2r} - \text{sign}(Q_B)|Q_B - Q_A|)$$

where B_B = coefficient (s/m^2); and C_B and U_B = constants (m).

Eqs. (13) and (14) are solved for Q_P and H_P at each pipe's interior and end nodes (i.e., junctions). Thus, two types of solutions are needed: interior analyses solve for the interior pipe hydraulics, and junction analyses consider adjacent pipe ends. Pumps and valves are omitted herein, for the topic of this study is the propagation of pressure waves along pipes. Instead, the reader is referred to standard references (e.g., Chaudhry 2014).

Interior and Junction Analyses

Interior analyses concern the black nodes shown in Fig. 1(b). There are only two unknowns, Q_P and H_P, and two compatibility equations, one for each adjacent reach [Fig. 3(a)], so solutions can be readily obtained. Because $\theta > 0$ may be used, a nonlinear solution technique is needed. Applying the Newton-Raphson method to the sum of Eq. (13) and (14) yields

$$Q_P^{(m+1)} = (J^{(m)})^{-1}(2\theta K_P^{(m)}|Q_P^{(m)}|Q_P^{(m)} + C_A + C_B) \tag{15}$$

$$J^{(m)} = 4\theta K_P^{(m)}|Q_P^{(m)}| + (2+k)B + (1-\theta)\varepsilon(K_A|Q_A| + K_B|Q_B|)$$

where $J^{(m)}$ = Jacobian (s/m^2); and $m+1$ and m = current and previous solution iterate indices, respectively. By repeatedly solving Eq. (15) for Q_P until $|Q_P^{(m+1)} - Q_P^{(m)}|/|Q_P^{(m+1)}| < e_{tol}$, in which e_{tol} is an error tolerance, a solution is found. The head H_P is then obtained from Eq. (13) or (14). If $\theta = 0$, then the compatibility equations are linear, and only a single iteration is needed.

Junction analyses compute the hydraulics at pipe end nodes [shown as the white filled nodes in Fig. 1(b)]. For an arbitrary junction i with $N_{A_{(i)}} + N_{B_{(i)}}$ adjacent pipes [Fig. 3(b)], the associated $N_{A_{(i)}} + N_{B_{(i)}}$ compatibility expressions are combined with one for nodal continuity to solve for $H_{(i)}$. Unlike interior analyses, a more efficient predictor-corrector scheme is used. The initial (predictor) head estimate for a junction i is

$$H_{(i)} = \left(\sum_{j\in N_{A_{(i)}}} \frac{1}{B_{A_{(j)}}} + \sum_{j\in N_{B_{(i)}}} \frac{1}{B_{B_{(j)}}}\right)^{-1} \times \left(\sum_{j\in N_{A_{(i)}}} \frac{C_{A_{(j)}}}{B_{A_{(j)}}} - \sum_{j\in N_{B_{(i)}}} \frac{C_{B_{(j)}}}{B_{B_{(j)}}} - q_{(i)}\right) \tag{16}$$

where $q_{(i)}$ = outflow or demand (m^3/s); $N_{A_{(i)}}$ and $N_{B_{(i)}}$ = collections of the link indices for pipes that end (with positive characteristic lines) and start (with negative characteristic lines) at node i, respectively; and the terms B_A, B_B, C_A, and C_B are computed using $\theta = 0$.

Once the predictor solution is calculated, initial flow estimates for the adjacent pipes are obtained from the appropriate compatibility expressions. Then, the final (corrector) solution is computed from Eq. (16) using the predictor flow estimates and actual θ. Nodal outflows may be demand-driven, pressure-dependent, or mixed (see Jung et al. 2009); in such cases, initial and updated estimates of $q_{(i)}$ can be used with the predictor and corrector steps, respectively. As with interior analyses, if $\theta = 0$ for all pipes adjacent to node i and $q_{(i)}$ is demand-driven, it follows that only the predictor junction analysis step needs to be performed because the compatibility equations are linear in Q_P. For reference, implementation algorithms for Eqs. (15) and (16) are presented in Appendix S1.

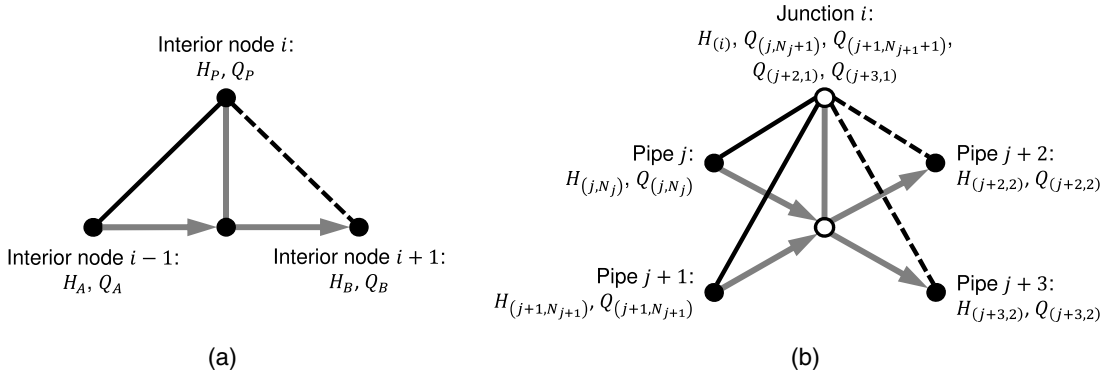

Fig. 3. Characteristic lines for hydraulic solutions at interior and end nodes: (a) interior node and adjacent reaches; (b) adjacent pipe reaches at a junction

J. Hydraul. Eng., 2018, 144(7): 04018031

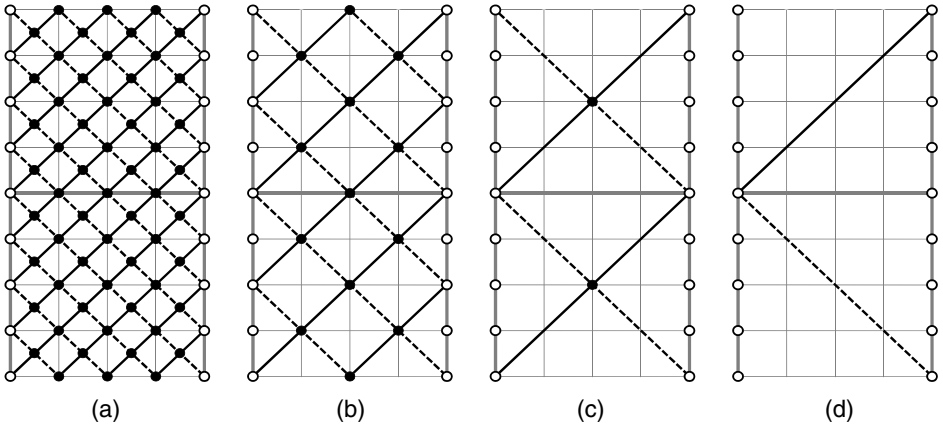

Fig. 4. Staggered variable reach computational grids for a pipe with $N_0 = 4$ base reaches: (a) $N_R = 8$ interior reaches; (b) $N_R = 4$ interior reaches; (c) $N_R = 2$ interior reaches; (d) $N_R = 1$ interior reach

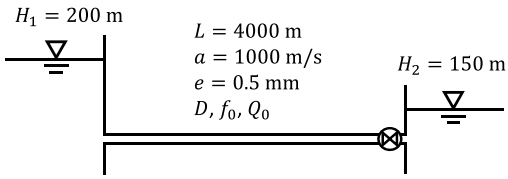

Parameter	Scenario 1	Scenario 2
R	0.25	1
D (mm)	345.1	42.4
Q_0 (m³/s)	1.84×10^{-1}	6.93×10^{-4}
f	0.0220	0.0432

Fig. 5. Example 1: idealized reservoir-pipeline-valve system

Before Eqs. (15) and (16) can be applied, the parameters N_R, θ, and ε are needed. The first-order fixed grid MOC uses $N_R = N_0$ and $\theta = \varepsilon = 0$, meaning hydraulic solutions are computed at each interior node. Large N_R is not always necessary though if a similar solution can be obtained more efficiently by using fewer interior reaches. Often this involves increasing Δt; though, for pipe networks, increasing Δt may result in too coarse of a discretization for some pipes. Instead, θ and ε can be selected for individual pipes with $N_R \neq N_0$.

Variable Reach Scheme

To balance the competing demands of numerical accuracy and computational efficiency, a variable reach scheme (where $N_R \neq N_0$ is permissible) was presented to select N_R, θ, and ε for individual pipes. Essentially, a pipe discretized with N_0 interior reaches $C = 1$, and a uniform computational grid can be modeled using any $N_R \in [2, Z(N_0), 2N_0]$, in which $Z(N_0)$ denotes the factors of N_0. For example, Fig. 4 shows the possible grids for a pipe with $N_0 = 4$; the staggered grids differ, but the same Δt is used to maintain compatibility with adjacent boundary conditions. Values of $\theta = \varepsilon = 0$ may suffice for the finer grids [Figs. 4(a and b)]. Comparatively, the coarser grids [Figs. 4(c and d)] are characterized by lower accuracy, meaning θ or $\varepsilon > 0$ are likely more appropriate.

Two error indices are presented to guide the selection of N_R, θ, and ε. Consider instantaneous valve closure at time $t = 0$ for the system shown in Fig. 5, which generates a pressure wave that propagates away from the valve. The head rise at the valve due to the flow change ΔQ is given by the Joukowsky equation as $\Delta H = -B \cdot \Delta Q$, and from Eq. (13), the head solution upon valve closure immediately upstream of the valve is $H(t = 0) = C_A$. Neglecting unsteady friction effects, which are typically less important than quasi-steady friction effects in the absence of high-frequency hydraulic variations, the relative error on ΔH is approximately

$$\epsilon_1 = (1 - W)\psi \tag{17}$$

where $W = (1 - \theta)(1 - \varepsilon)$ = weighting factor. Following the valve's closure, $H(t)$ will increase until it reaches a maximum at time $T = 2L/a$, at which point the reflected wave front returns. The positive compatibility equation can be used to approximate $H(t)$ during this period as

$$H(t) \approx H_1 + B\left(1 + R\left(\frac{t}{T} - 1\right)\right)Q_0, \quad 0 \le t < T \tag{18}$$

A solution computed using N_R, θ, and ε will have a maximum head error of approximately $-2W\Delta t \cdot \partial H/\partial t$ (m), so the head extremum error relative to ΔH is

$$\epsilon_2 = -W\psi \tag{19}$$

Eqs. (17) and (19) characterize the solution error following sudden flow changes. A value of $\epsilon_1 > 0$ indicates overestimating $|\Delta H|$, and $\epsilon_2 < 0$ corresponds to underestimating the magnitude of the head extrema. While obtained for downstream flow changes along a single pipe, the expressions are equally representative of upstream flow changes if considered as absolute values; moreover, controlling the error associated with a single pipe also controls that for networks having multiple interconnected pipes.

If ϵ_1 and ϵ_2 are prescribed on the basis of acceptable levels of error, the minimum required N_R is

$$N_R \ge R \cdot \max\left\{\left|\frac{1 - W}{\epsilon_1}\right|, \left|\frac{W}{\epsilon_2}\right|\right\} \tag{20}$$

Eq. (20) directly relates the minimum number of interior reaches to the attenuation index R. This suggests that pipes having greater R should be modeled with greater N_R, which agrees with the work of others (Wylie and Streeter 1993; Ramalingam et al. 2009).

An efficient solution is obtained by minimizing the right hand side of Eq. (20), so θ and ε can be taken as any combination that satisfies

$$W = \frac{1}{E+1} \tag{21}$$

where $E = |\epsilon_1/\epsilon_2|$ = error tolerance ratio.

Together, the solutions [Eqs. (15) and (16)] and variable reach scheme [Eqs. (20) and (21)] form the GCM. The error tolerances are both simple and intuitive, and they can be chosen for individual pipes according to where greater accuracy is required. Consequently, larger N_R and more demanding implicit solutions are selectively provided only where needed, thereby facilitating efficient computations. While smaller ϵ_1 and ϵ_2 provide more accurate solutions, this comes at the expense of computational efficiency. Altogether, the aim of the GCM is to balance the competing demands of numerical accuracy and computational efficiency.

Computational Accounting

In addition to resolving the accuracy-efficiency tension, the generalized approach encompasses the other numerical methods. Accordingly, it can be implemented as either or a combination of the MOC, WCM, and AWH, which permits a direct comparison of their computational features. These are discussed below.

Comparison of Numerical Methods

Between the numerical methods, the two key differences are their computational space-time grids (determined by N_R) and their head loss treatments (represented by θ and ε). Consequently, the GCM reduces to each of the MOC, WCM, and AWH depending on N_R, θ, and ε. The first-order MOC computes hydraulic solutions at all interior nodes, so it is represented by $N_R = N_0$ and $\theta = \varepsilon = 0$. With $N_R = 2$, the GCM resembles the WCM by considering the midlength interaction of impinging pressure waves. Interior head losses are effectively grouped at a single interior node, the so-called friction orifice analogy—additional friction orifices are considered with the GCM by increasing N_R. Both first-order ($\theta = 1$, $\varepsilon = 0$) and second-order ($\theta = 0.5$, $\varepsilon = 0$) implicit approximations have been used with the WCM (Wood et al. 2005a; Ramalingam et al. 2009). Being a derivative of the MOC, AWH considers $\theta = \varepsilon = 0$ with $N_R = 1$ because interior analyses are omitted. Indeed, the methods' computational grids differ, yet each relies on characteristic lines that extend N_0/N_R time steps back from the solution step (Fig. 6).

While comparing the methods, it is worth further commenting on the GCM and the WCM. Although the generalized approach with $N_R = 2$ is fundamentally the same as the WCM, Eqs. (15) and (16) do not reduce to the solution expressions reported in the WCM literature for three reasons. First, the WCM uses opposite sign conventions for flows up and downstream of interior nodes, and Eqs. (15) and (16) additionally consider unsteady friction effects. More importantly, the methods' friction treatments differ: the GCM considers head losses at the intersection of the positive and negative characteristic lines, whereas the WCM concentrates head losses at interior orifice elements (Fig. 7). Nonetheless, these are merely numerical artefacts.

Indeed, the MOC, WCM, and AWH are profoundly similar. The only differences are their computational grids and friction treatments; otherwise, the methods represent wave propagation in the same manner and thus have similar solution approaches. This contrasts with claims that the MOC and WCM are fundamentally different (Wood et al. 2005b; Ramalingam et al. 2009). Differences between the numerical methods, however, do have implications for numerical accuracy and computational efficiency. Because the GCM can assume the form of each of the MOC, WCM, and AWH, it is used to study the methods' properties below.

Accuracy and Efficiency

Computational efficiency relates to the number of floating point operations (FLOPs) needed to obtain a solution. In turn, operation

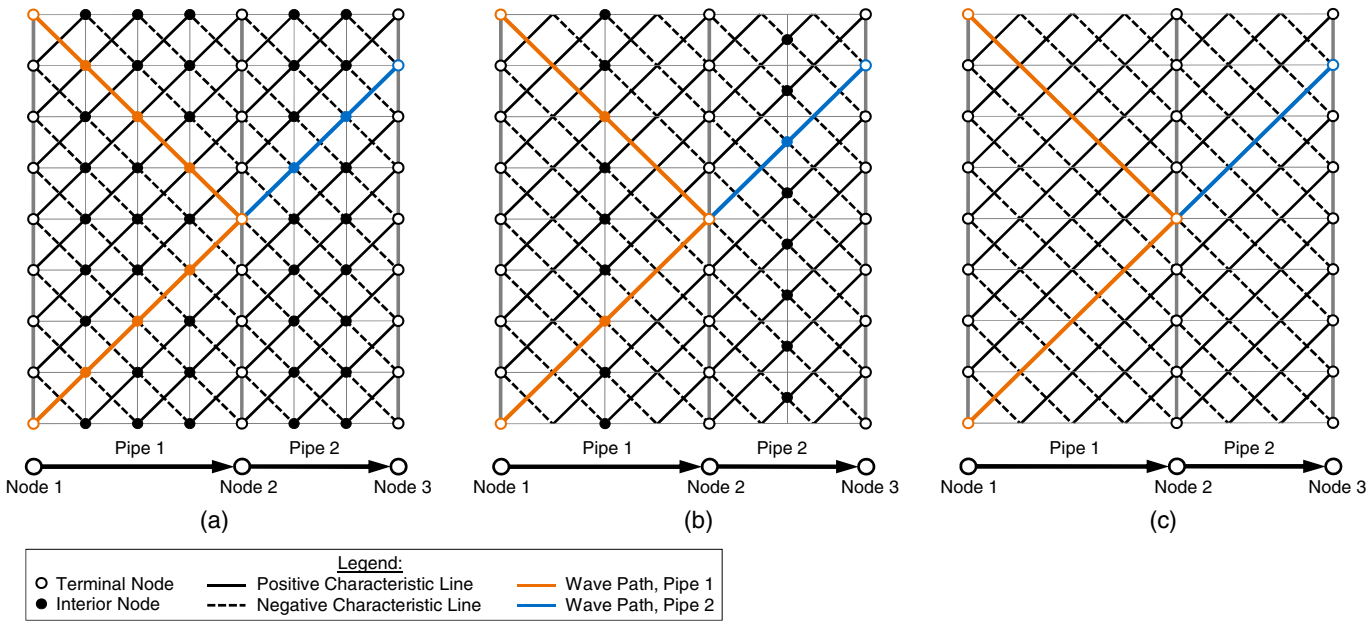

Fig. 6. Comparison of fixed space-time computational grids showing the solution nodes along a wave path arising from a disturbance at the start of Pipe 1: (a) method of characteristics; (b) wave characteristics method with one friction orifice; (c) algebraic water hammer

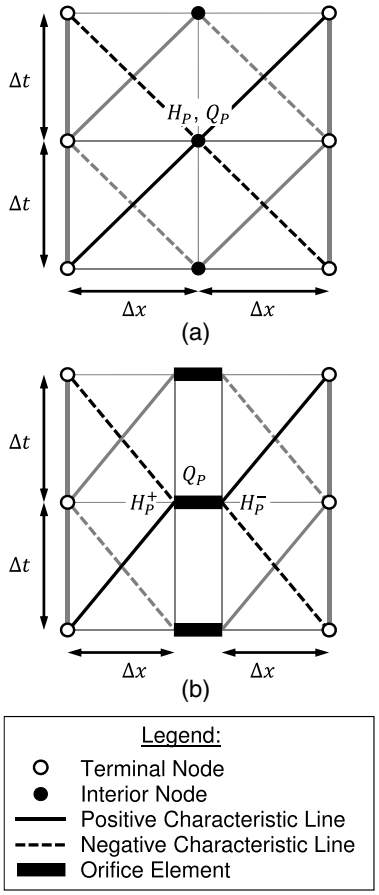

Fig. 7. Comparison of friction representations for a pipe modeled with $N_R = 2$: (a) characteristic methods with head losses distributed along characteristic lines; (b) wave characteristics method with head losses concentrated at an orifice element

counts for the generalized approach are affected by the computational grid (via N_R), θ, and ε. To assess these, Table 1 lists the interior analysis unit FLOPs for a single pipe (the number of FLOPs per interior node and time step) and the minimum required N_R [Eq. (20)] to provide solutions of comparable accuracy; similarly, the unit FLOPs for junction analyses (per pipe per time step) are reported in Table 2. The operation counts are closely based on the interior analysis implementation algorithm presented in Appendix S1.

Tables 1 and 2 illustrate how the solution unit operations and minimum required N_R vary with the configuration. Fixed θ and ε permit modest unit FLOP reductions; more so, the friction treatment largely affects computational effort. For a given θ and ε, an analysis using unsteady friction requires approximately twice as many unit FLOPs as one using steady friction. Additionally, computational effort (the product of the interior analysis unit FLOPs and $N_R - 1$) is equally affected by N_R, itself a function of θ and ε. Consider $[\theta, \varepsilon]$, $[\theta, \varepsilon = 0]$, and $[\theta = 0, \varepsilon]$. These configurations have similar minimum N_R for the same ϵ_1 and ϵ_2, so variable $[\theta, \varepsilon]$ is the least efficient treatment due to having the highest interior analysis unit FLOPs. Conversely, $[\theta = 0, \varepsilon]$ is the most efficient while providing comparable flexibility. Key here is that particular reductions permit gains in efficiency without sacrificing numerical accuracy.

Also of interest are the first-order MOC ($\theta = \varepsilon = 0$) and second-order WCM ($\theta = 0.5$, $\varepsilon = 0$) representations. If configured to match ϵ_2 for the MOC (with $N_R = N_0$), the WCM requires

Table 1. Interior Analysis Unit FLOPs for the Generalized Characteristic Method

			Friction treatment (FLOPs/pipe-node-time step)		
θ	ε	Minimum N_R	Unsteady	Quasi-steady	Steady
θ[a]	ε	$R \cdot \max\left(\left\lvert\frac{1-W}{\varepsilon_1}\right\rvert, \left\lvert\frac{W}{\varepsilon_2}\right\rvert\right)$	103	86	51
θ[a]	0	$R \cdot \max\left(\left\lvert\frac{\theta}{\varepsilon_1}\right\rvert, \left\lvert\frac{\theta-1}{\varepsilon_2}\right\rvert\right)$	98	81	46
0.5[a]	0	$\frac{1}{2}R \cdot \max\left(\left\lvert\frac{1}{\varepsilon_1}\right\rvert, \left\lvert\frac{1}{\varepsilon_2}\right\rvert\right)$	89	72	37
1[a]	0	$R/\lvert\varepsilon_1\rvert$	93	76	41
0	ε	$R \cdot \max\left(\left\lvert\frac{\varepsilon}{\varepsilon_1}\right\rvert, \left\lvert\frac{\varepsilon-1}{\varepsilon_2}\right\rvert\right)$	54	34	20
0	0.5	$\frac{1}{2}R \cdot \max\left(\left\lvert\frac{1}{\varepsilon_1}\right\rvert, \left\lvert\frac{1}{\varepsilon_2}\right\rvert\right)$	52	32	18
0	1	$R/\lvert\varepsilon_1\rvert$	48	28	14
0	0	$R/\lvert\varepsilon_2\rvert$	47	27	13

[a]Assuming three solution iterations.

Table 2. Junction Analysis Unit FLOPs for the Generalized Characteristic Method

		Friction treatment (FLOPs/pipe-time step)		
θ	ε	Unsteady	Quasi-steady	Steady
θ	ε	138	106	72
θ	0	134	98	64
0.5	0	134	98	64
1	0	130	94	60
0	ε	116	80	46
0	0.5	114	78	44
0	1	110	74	40
0	0	110	74	40

$N_R = N_0/2$; thus, the WCM features fewer interior analysis operations for unsteady and quasi-steady friction. In the case of steady friction, however, the MOC requires fewer interior analysis FLOPs when $N_0 > 10$. These remarks do not imply that one method is always more accurate and efficient than the other—such inferences are subject to the specific implementations (which here are based on Appendix S1) as well as computational effort for junction analyses. Certainly, these discussions are insightful, but the numerical methods' performance is best compared via example.

Unified Simulation of Transient Flow

Three examples demonstrate the current work. The first, a simple pipeline, tests the performance of the generalized approach for different configurations, and the other two examples emphasize more complex networks. In each case, the method of specified time intervals was used with suitable Δt that minimizes or avoids the need for length and wave speed adjustments. Further, the WCM was implemented with $N_R = 2$ for simplicity. Vapor cavity formation due to excessive negative pressures was also neglected in this study because the objective is to contrast the numerical methods.

Example 1: Valve Closure

Unsteady flow analyses are often conducted to estimate the extreme pressures and frequency response resulting from boundary changes. To explore how the generalized solution performed in these respects, instantaneous valve closure was simulated for the system in Fig. 5 using the generalized method with different N_R, θ, and ε. A comparison of the relative head extrema error against ψ (Fig. 8) illustrates how a finer discretization yields smaller error; further, Fig. 8 shows that for the same ψ and R, implicit schemes ($\theta > 0$ or $\varepsilon > 0$) better predict the maximum head than first-order explicit approximations. This was because $\theta = \varepsilon = 0$ overestimates the friction integral, thereby underestimating the head extrema. Moreover, the results compare well against the ε_2 contours at low R. This suggests that Eq. (18) is rather a reasonable approximation. As R increases though, the error diverges from that predicted by Eq. (19) due to greater pressure wave attenuation, so the contours provide a conservative overestimate. In addition to the maximum head error, solution resolution is also key.

Adequate solution resolution is necessary to represent frictional pressure wave attenuation. Consider the head predicted upstream of the valve following sudden valve closure (Fig. 9). The first-order explicit MOC uses $N_R = 25$, the GCM here is based on the variable reach scheme with $\epsilon_1 = \epsilon_2 = 1\%$ (yielding $N_R = 13$), and the WCM considers a second-order implementation with $N_R = 2$. Because the WCM uses lower N_R, it produces the lowest resolution solution with a maximum head error of -6%. Setting $\theta = 1$ would resolve the latter issue, but the solution resolution can only be improved by increasing N_R at the expense of greater computational effort. The results for the MOC and generalized approach, however, are in much better agreement with the numerically converged solutions due to using sufficiently large N_R; in fact, their maximum head errors (-0.9% for the MOC and -1.0% for the generalized method) compare well with $|\epsilon_2| = 1\%$, as predicted by Fig. 8(a). The key is that the solution error and resolution can be controlled by selecting suitable ϵ_1 and ϵ_2 for the GCM.

Example 2: Looped Pipe Network

In addition to frictional attenuation, the transient hydraulics of pipe networks are largely affected by the interaction and reflection of waves. With this in mind, Example 2 compares the numerical methods as used to simulate sudden valve closure for a small looped pipe network (Fig. 10) (Streeter and Wylie 1967); the system properties can be readily found in Wood et al. (2005b). Pipe length adjustments are minimized to less than 2% by using $\Delta t = 0.02$ s, and the GCM here is based on $\epsilon_1 = \epsilon_2 = 1\%$.

Though the numerical methods differ, their results for the valve's upstream head are similar (Fig. 11). This is a result of the system response being predominantly governed by the interaction and reflection of waves rather than their attenuation; accordingly, the MOC, WCM, AWH, and generalized method yield comparable results because they have similar junction analyses.

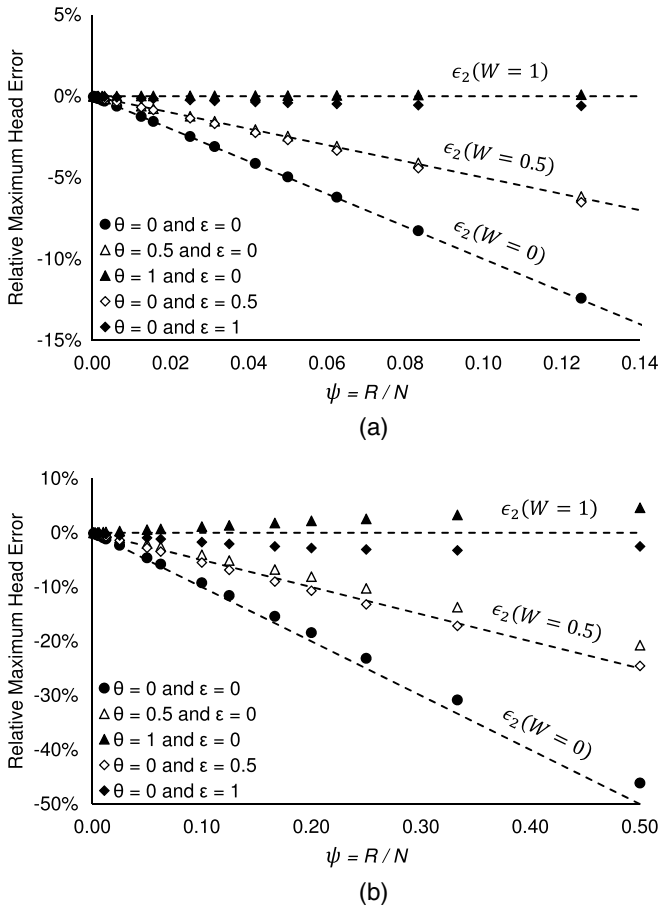

Fig. 8. Relative head extrema error for Example 1 using the generalized solution: (a) results for $R = 0.25$; (b) results for $R = 1$

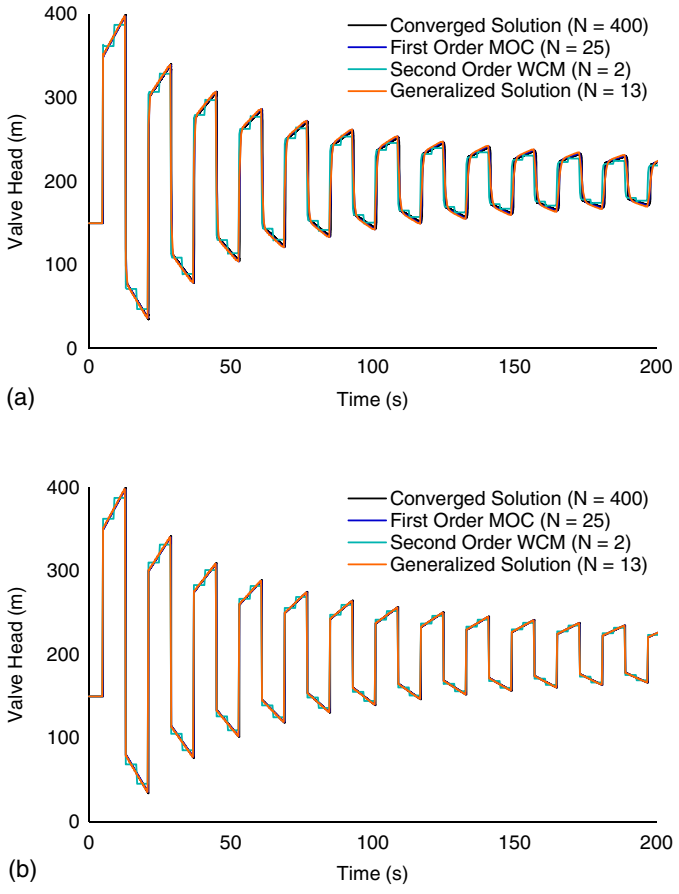

Fig. 9. Comparison of simulation results for Example 1 with $R = 0.25$: (a) results using unsteady friction; (b) results using quasi-steady friction

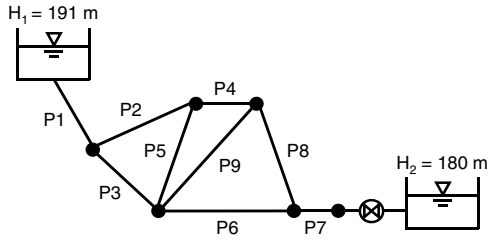

Fig. 10. Example 2 pipe network (adapted from Streeter and Wylie 1967)

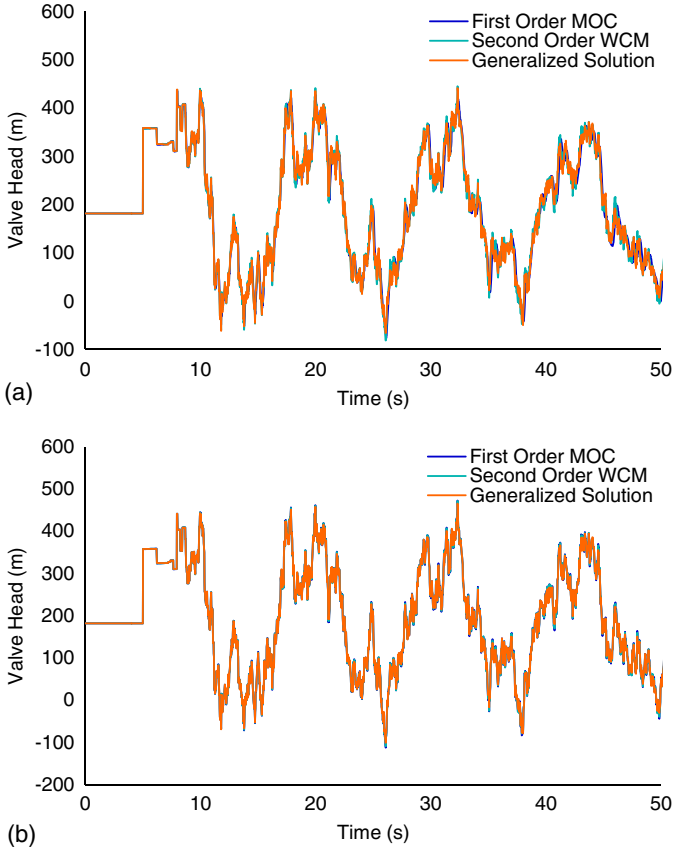

Fig. 11. Comparison of Example 2 results for the head at the valve following instantaneous valve closure: (a) results using unsteady friction; (b) results using quasi-steady friction

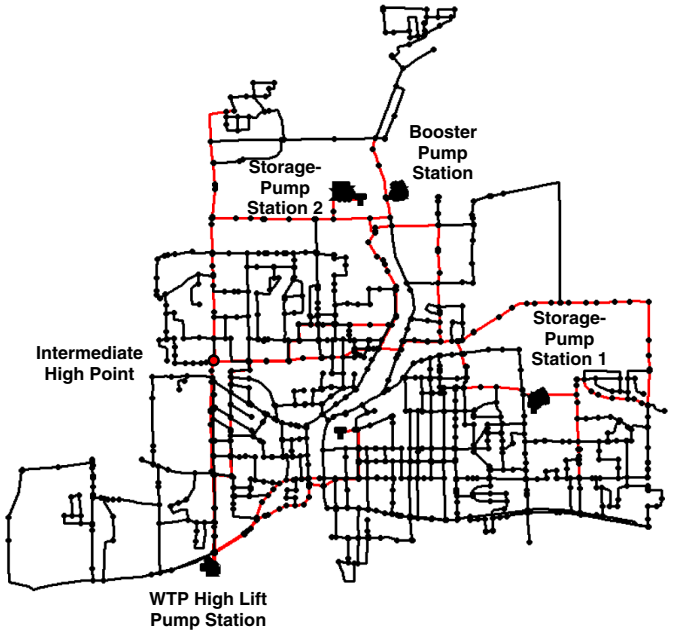

Fig. 12. Example 3 water distribution system showing transmission network in red

Indeed, Fig. 11 does show minor variations between the solutions when unsteady friction effects were considered, a result of differing N_R. Not only does N_R affect the solution resolution, it also affects the finite difference approximations of $\partial Q/\partial t$ and $\partial Q/\partial x$. Key here is to adequately capture unsteady energy dissipation, but the differences are of little importance for practical purposes.

Regarding computational performance, Table 3 summarizes the methods' solution FLOPs per time step. Individual pipes were modeled with $N_R = 1$ using the GCM, meaning it has zero interior analysis FLOPs for both friction treatments. Of the three numerical methods, the MOC features the greatest computational effort; in fact, it required more than 10 times more FLOPs than the GCM, a significant amount. Despite these differences, the three methods provide similar results, with the generalized solution (having the fewest FLOPs) being the most practical.

Example 3: Water Distribution System

Example 3 compares the numerical approaches for a more practical application, simulating a power failure event in a WDS (Fig. 12). An average demand of 25 ML/day is supplied by the

Table 3. Example 2 Solution FLOPs per Time Step and Relative Run Times

Friction treatment	Solution method	$\overline{N_R}$	Computations (FLOPs/time step)			Relative run time (%)
			Interior analysis	Junction analysis	Total	
Unsteady	GCM ($\theta = 0$)	1.0	0	1,040	1,040	8.1
	WCM (second order)	2.0	800	1,210	2,010	25.8
	MOC (first order)	29.2	11,900	990	12,890	100.0
Quasi-steady	GCM ($\theta = 0$)	1.0	0	720	720	7.0
	WCM (second order)	2.0	650	880	1,530	26.5
	MOC (first order)	29.2	6,900	670	7,600	100.0
Steady	GCM ($\theta = 0$)	1.0	0	410	410	8.1
	WCM (second order)	2.0	330	580	910	30.0
	MOC (first order)	29.2	3,300	360	3,660	100.0

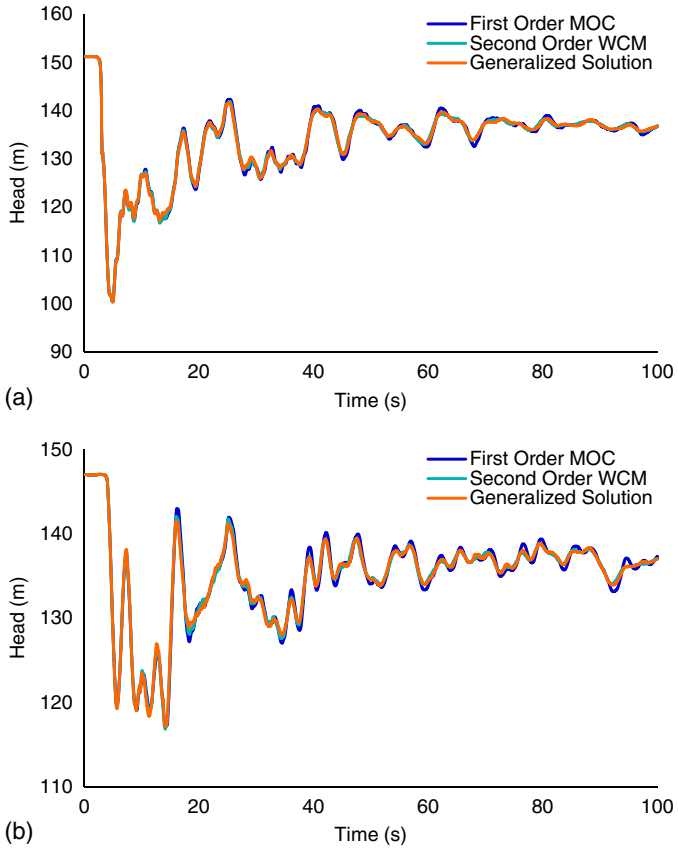

Fig. 13. Example 3 simulation results with unsteady friction and $\Delta t = 0.02$ s: (a) head at the high-lift pump station discharge; (b) head at the intermediate high point

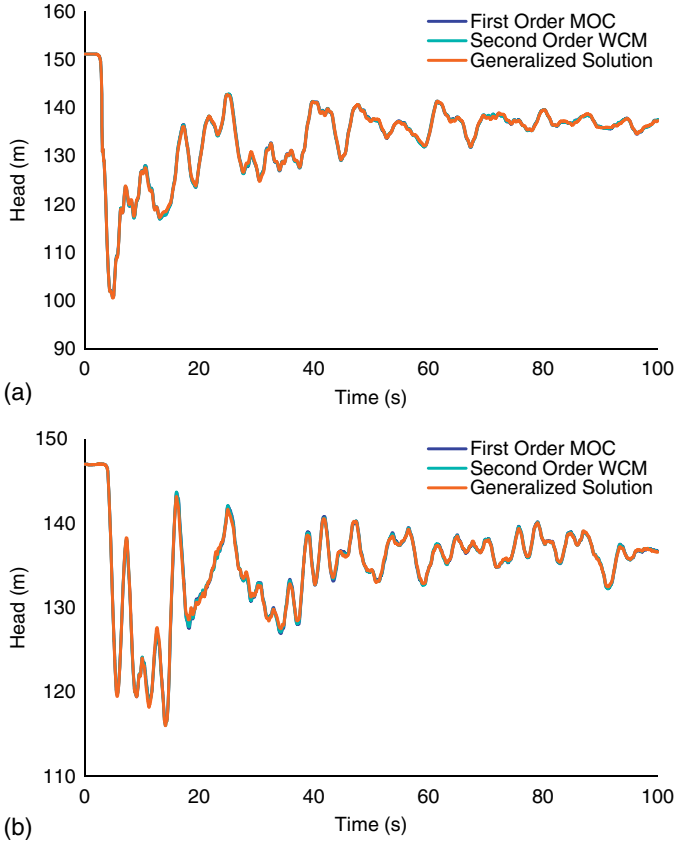

Fig. 14. Example 3 simulation results with steady friction and $\Delta t = 0.02$ s: (a) head at the high-lift pump station discharge; (b) head at the intermediate high point

system through four pump stations, the primary of which is a high-lift facility at a water treatment plant. The model comprises 1,490 pipes and 1,310 junctions (see Appendix S2). For this example, pipes with diameters greater than 400 mm (which typically comprise rigid materials, such as concrete and steel) were assigned $a = 1{,}050$ m/s, and the remaining smaller pipes, often constructed using flexible (polymeric) materials, were assigned $a = 350$ m/s. Unlike rigid pipes, flexible pipes typically exhibit viscoelastic deformation effects under highly dynamic conditions. However, this was omitted from the current work for simplicity. Power failures are often the most problematic event for WDSs; following the loss of power to a pump, rapid flow deceleration gives rise to highly dynamic conditions. Here study, the event of interest is a local power failure at the high-lift pump station.

Simulation results from the numerical methods are shown in Figs. 13 and 14. A time step of $\Delta t = 0.02$ s was used due to the otherwise rather high computational cost of using the MOC for a large model. With $\epsilon_1 = \epsilon_2 = 1\%$ and $\theta = 0$, over 90% of the WDS is modeled with $N_R = 1$ for the GCM, whereas the MOC results are based on an average $N_R = 15$. Despite such differences, Figs. 13 and 14 show that the numerical methods yield comparable solutions with only minor variations, again because the system's response is dominated by pressure wave interaction and reflection. The methods' solution FLOPs and computational run times, however, differ significantly (Table 4). Those for the GCM are less than the solution FLOPs for even the WCM for both friction treatments, making it the preferred alternative.

Practical Considerations

Examples 1–3 demonstrate the superior performance of the generalized approach. Although effective, the variable reach scheme has two shortcomings: Eq. (20) does not consider solution stability or unsteady friction, and using $\varepsilon = 0$ may inadvertently zero the friction integral (Liou and Wylie 2014). These can be addressed by restricting the maximum ϵ_1, ϵ_2, and E, thereby forcing an implicit friction treatment (with greater stability properties; see Chaudhry and Hussaini 1985) and larger N_R. Simultaneously, larger N_R also benefit numerical accuracy for unsteady friction. An indicator specific to this would help, but a detailed assessment is beyond the scope of this manuscript. If a pipe, however, is still modeled with $N_R = 1$, zeroing the friction integrals is not a major concern, for only pipes with low R and, thus, low attenuation potential are represented by $N_R = 1$. A minimum N_R can even be adopted (much like the WCM in which $N_R \geq 2$). Even without the aforementioned numerical artefacts, the test cases show that the solutions from the MOC and generalized approach are quite similar.

Considering the approaches' underlying differences, it is also worth discussing why the generalized method compares well. The answer relates to the adaptive variable reach scheme and, more broadly, the fact that most networks have pipes of low R. For Example 1, the system response is predominantly governed by frictional attenuation and thus R. Because the generalized method used sufficiently large N_R (according to the variable reach scheme), it adequately represents attenuation, whereas the WCM

Table 4. Example 3 Solution FLOPs per Time Step and Relative Run Times

Friction treatment	Solution method	$\overline{N_R}$	Computations (FLOPs/time step)			Relative run time (%)
			Interior analysis	Junction analysis	Total	
Unsteady	GCM ($\theta = 0$)	1.4	28,800	173,000	202,000	13.9
	WCM (second order)	2.0	133,000	200,000	333,000	19.5
	MOC (first order)	14.7	956,000	164,000	1,120,000	100.0
Steady	GCM ($\theta = 0$)	1.4	10,700	68,500	79,200	11.5
	WCM (second order)	2.0	55,100	95,300	150,000	19.4
	MOC (first order)	14.7	264,000	59,600	324,000	100.0

(with $N_R = 2$) does not. Unlike Example 1, Examples 2 and 3 concern the more common case of networks with pipes having low R. Thus, attenuation primarily arises from pressure wave dispersion and demanded relief rather than friction; consequently, lower N_R can be used. It is for this reason that the generalized method and WCM compare well against the MOC, even though they used much lower N_R.

Like the generalized approach, the WCM also uses varying N_R via friction orifices. Though similar, the current work features a number of distinct advantages: N_R is chosen according to ϵ_1 and ϵ_2 rather than heuristics (as in Ramalingam et al. 2009), a variable quasi-steady friction treatment is used, and $N_R = 1$ is permissible. Additionally, unsteady friction is neglected in the WCM literature, but not here, and the GCM solution equations may be reduced for $\theta = 0$ and variable ε to achieve further computational savings with negligible change in accuracy. The main advantage of the GCM is its generality, namely that it can be implemented as either or a combination of the MOC, WCM, and AWH.

Conclusions

Practical unsteady flow modeling requires solution methods that are both numerically accurate and computationally efficient. To balance these competing demands, a novel generalized methodology was developed by combining a flexible friction approximation with the variable reach scheme. These allow individual pipes to be modeled according to the required solution accuracy; in this way, larger N_R and higher order friction approximations are only used where needed, thereby facilitating accurate and efficient simulations. Owing to its generality, the present approach encompasses each of the MOC, the WCM, and AWH. From this, the characteristic methods are fundamentally similar, with the only differences being N_R, θ, ε, and, consequently, their computational efficiency. Altogether, the generalized method provides a means of balancing the accuracy-efficiency tension.

Three examples elucidated the current approach. The first explores how N_R affects the solution accuracy and solution resolution for a pipeline system, while the remaining examples concern more complex networks in which both numerical accuracy and computational efficiency are key. Even considering unsteady friction, the numerical methods compare well for the pipe networks. And yet, their computational performance, evaluated using interior analysis operation counts, differs significantly. In each case, the generalized method requires fewer computations while providing comparable results, a distinct advantage over its alternatives. Ultimately, models are an approximation of reality, so simplifications that permit efficient analyses while adequately representing the underlying physics, such as in this study, certainly merit consideration.

Acknowledgments

For their financial support, the authors thank the National Sciences and Engineering Research Council of Canada and FP&P HydraTek. The three anonymous reviewers and associated editor also are thanked for their feedback, review comments, and discussions, each of which contributed to a much improved article.

Notation

The following symbols are used in this paper:

A = pipe area (m^2);
a = wave speed (m/s);
B = pipe compressibility constant (s/m^2);
B_A and B_B = compatibility equation coefficients (s/m^2);
C = CFL number;
C_A and C_B = compatibility equation constants (m);
D = pipe diameter (m);
E = error tolerance ratio;
f = friction factor;
g = acceleration due to gravity (m/s^2);
H = head (m);
J_{QF} = quasi-steady friction unit head loss;
J_{UF} = unsteady friction unit head loss;
K = resistance coefficient (s^2/m^5);
k = shear decay coefficient;
L = pipe length (m);
N_{A_i} and N_{B_i} = collection of indices for pipes adjacent to junction i;
N_R = number of modeled interior reaches;
N_0 = number of discretized interior reaches;
Q = flow (m^3/s);
q = junction outflow (m^3/s);
R = pipe attenuation index;
R = Reynolds number;
r = reach back index;
t = time (s);
U_A and U_B = compatibility equation constants (m);
W = integration weighting factor;
x = longitudinal distance (m);
ΔH = potential surge (m);
Δt = time step (s);
Δx = reach length (m);
ε = friction integration parameter;
ϵ_1 = head rise relative error;
ϵ_2 = extreme head relative error;
θ = friction integration parameter; and
ψ = pipe reach attenuation index.

Supplemental Data

The GCM implementation algorithms and the Epanet input file for Example 3 are available online in the ASCE Library (www.ascelibrary.org).

References

Boyd, G. R., et al. (2004). "Intrusion within a simulated water distribution system due to hydraulic transients. II: Volumetric method and comparison of results." *J. Environ. Eng.*, 10.1061/(ASCE)0733-9372(2004)130:7(778), 778–783.

Brunone, B., Golia, U. M., and Greco, M. (1991). "Some remarks on the momentum equation for fast transients." *Int. Meeting on Hydraulic Transients with Column Separation, 9th Round Table*, International Association for Hydraulic Research, Valencia, Spain, 201–209.

Chaudhry, M. H. (2014). "Transient flow equations." Chapter 2, *Applied hydraulic transients*, 3rd Ed., Springer, New York, 35–64.

Chaudhry, M. H., and Hussaini, M. Y. (1985). "Second-order accurate explicit finite difference schemes for waterhammer analysis." *J. Fluid Eng.*, 107(4), 523–529.

Ebacher, G., Besner, M-C., Lavoie, J., Jung, B. S., Karney, B. W., and Prévost, M. (2011). "Transient modeling of a full-scale distribution system: Comparison with field data." *J. Water Resour. Plann. Manage.*, 10.1061/(ASCE)WR.1943-5452.0000109, 173–182.

Ferrante, M., Brunone, B., and Meniconi, S. (2009). "Leak detection in branched pipe systems coupling wavelet analysis and a Lagrangian model." *J. Water Supply Res.*, 58(2), 95–106.

Friedman, M., et al. (2004). *Verification and control of pressure transients and intrusion in distribution systems*, American Water Works Association Research Foundation, Denver.

Holloway, M. B., and Chaudhry, M. H. (1985). "Stability and accuracy of waterhammer analysis." *Adv. Water Resour.*, 8(3), 121–128.

Huang, Y., Duan, H.-F., Zhao, M., Zhang, Q., Zhao, H., and Zhang, K. (2017). "Transient influence zone based decomposition of water distribution networks for efficient transient analysis." *Water Resour. Manage.*, 31(6), 1915–1929.

Jung, B. S., Boulos, P. F., and Altman, T. (2011). "Optimal transient network design: A multi-objective approach." *J. AWWA*, 103(4), 118–128.

Jung, B. S., Boulos, P. F., and Wood, D. J. (2009). "Effect of pressure-sensitive demand on surge analysis." *J. AWWA*, 101(4), 100–111.

Kim, S. (2007). "Impedance matrix method for transient analysis of complicated pipe networks." *J. Hydraul. Res.*, 45(6), 818–828.

León, A., Ghidaoui, M., Schmidt, A., and García, M. (2008). "Efficient second-order accurate shock-capturing scheme for modeling one- and two-phase water hammer flows." *J. Hydraul. Eng.*, 10.1061/(ASCE)0733-9429(2008)134:7(970), 970–983.

Liou, C., and Wylie, E. (2014). "Approximation of the friction integral in water hammer equations." *J. Hydraul. Eng.*, 10.1061/(ASCE)HY.1943-7900.0000869, 06014008.

Nault, J. D., Karney, B. W., and Jung, B. S. (2016). "Algebraic water hammer: Global formulation for simulating transient pipe network hydraulics." *World Environmental and Water Resources Congress 2016*, EWRI, West Palm Beach, FL, 191–201.

Ramalingam, D., Lingireddy, S., and Wood, D. J. (2009). "Using the WCM for transient modeling of water distribution networks." *J. AWWA*, 101(2), 75–89.

Streeter, V. L., and Wylie, E. B. (1967). *Hydraulic transients*, McGraw-Hill, New York.

Vardy, A. E., and Brown, J. M. B. (1996). "On turbulent, unsteady, smooth-pipe flow." *Proc., Int. Conf. on Pressure Surges and Fluid Transients*, BHR Group, Harrogate, U.K., 289–311.

Vítkovský, J. P., Bergant, A., Simpson, A. R., and Lambert, M. F. (2006). "Systematic evaluation of one-dimensional unsteady friction models in simple pipelines." *J. Hydraul. Eng.*, 10.1061/(ASCE)0733-9429(2006)132:7(696), 696–708.

Vítkovský, J. P., Lambert, M., Simpson, A., and Bergant, A. (2000). "Advances in unsteady friction modelling in transient pipe flow." *Proc., 8th Int. Conf. on Pressure Surges*, BHR, Hague, Netherlands.

Vítkovský, J. P., Lee, P. L., Zecchin, A. C., Simpson, A. R., and Lambert, M. F. (2011). "Head- and flow-based formulations for frequency domain analysis of fluid transients in arbitrary pipe networks." *J. Hydraul. Eng.*, 10.1061/(ASCE)HY.1943-7900.0000338, 556–568.

Wood, D. J. (2005). "Waterhammer analysis—Essential and easy (and efficient)." *J. Environ. Eng.*, 10.1061/(ASCE)0733-9372(2005)131:8(1123), 1123–1131.

Wood, D. J., Dorsch, R. G., and Lightner, C. (1966). "Wave plan analysis of unsteady flow in closed conduits." *J. Hydraul. Div.*, 92(2), 83.

Wood, D. J., Lingireddy, S., and Boulos, P. F. (2005a). "The wave characteristic method." Chapter 2, *Pressure wave analysis of transient flow in pipe distribution systems*, MWH Software, Pasadena CA, 2.1–2.36.

Wood, D. J., Lingireddy, S., Boulos, P. F., Karney, B. W., and McPherson, D. L. (2005b). "Numerical methods for modeling transient flow in distribution systems." *J. AWWA*, 97(7), 104–115.

Wylie, E. B. (1983). "The microcomputer and pipeline transients." *J. Hydraul. Eng.*, 10.1061/(ASCE)0733-9429(1983)109:12(1723), 1723–1739.

Wylie, E. B., and Streeter, V. L. (1978). "Solution by characteristics method." Chapter 3, *Fluid transients*, McGraw-Hill, New York, 31–65.

Wylie, E. B., and Streeter, V. L. (1993). *Fluid transients in systems*, Prentice-Hall, Englewood Cliffs, NJ.

Zecchin, A. C., Lambert, M. F., Simpson, A. R., and White, L. B. (2010). "Frequency-domain modeling of transients in pipe networks with compound nodes using a Laplace-domain admittance matrix." *J. Hydraul. Eng.*, 10.1061/(ASCE)HY.1943-7900.0000248, 739–755.

Zhao, M., and Ghidaoui, M. (2004). "Godunov-type solutions for water hammer flows." *J. Hydraul. Eng.*, 10.1061/(ASCE)0733-9429(2004)130:4(341), 341–348.

Zielke, W. (1968). "Frequency-dependent friction in transient pipe flow." *J. Basic Eng.*, 90(1), 109–115.